Electronic Supplementary Information (ESI) for: Structural and mechanical characteristics of exosomes from osteosarcoma cells explored by 3D-atomic force microscopy

Ayhan Yurtsever,[*,†] Takeshi Yoshida,[†,‡] Arash Badami Behjat,[†] Yoshihiro Araki,[‡,¶] Rikinari Hanayama,[†,‡] and Takeshi Fukuma[*,†]

†*WPI Nano Life Science Institute (WPI-Nano LSI), Kanazawa University, Kakuma-machi, Kanazawa 920-1192, Japan*

‡*Department of Immunology, Kanazawa University Graduate School of Medical Sciences, 13-1 Takara, Kanazawa, Ishikawa 920-8640, Japan*

¶*Department of Orthopaedic Surgery, Kanazawa University Graduate School of Medical Sciences, 13-1 Takara, Kanazawa 920-8640, Japan*

E-mail: yurtsever@staff.kanazawa-u.ac.jp; fukuma@staff.kanazawa-u.ac.jp

Phone: +81-76-234-4564. Fax: +81-76-234-4632

Supplementary Materials and Methods

Nanoparticle tracking analysis (NTA)

The size distribution and particle concentration of purified exosomes were analyzed using a NanoSight LM10 system (Malvern Panalytical, UK) equipped with particle-tracking software and a red (642 nm) laser. Briefly, exosomes isolated from each cell line were diluted by 100- to 1000-fold with PBS to the appropriate concentration for the analysis, a range from 1 to 10 $\times 10^8$ particles/mL. All acquisition settings, including capture time, camera level, and detection threshold, were kept the same in all samples to minimize variability. For each sample, the measurements were performed in triplicate under identical analysis settings. The results of these three measurements were then averaged to obtain the exosomes concentration and their size distribution (Figure S1). The mean diameter of exosomes determined by NTA is larger than that obtained by AFM and TEM measurements. This difference can be attributed to the fact that NTA measures the hydrodynamic radius. The hydrodynamic sizes of exosomes are larger than their geometric sizes.[1] For the TEM measurements, this could be due to the vesicle's dehydration by the staining process. This could lead to smaller sizes for exosomes in TEM measurements than the sizes determined by NTA measurements.

Negative-staining transmission electron microscopy (TEM)

The morphology of isolated exosomes was additionally confirmed by transmission electron microscopy (TEM). Exosomes (1×10^{10} particles) isolated from each cell line were placed onto carbon-coated copper grids, and allowed to be absorbed onto the grid for 3 min. After being rinsed with distilled water to remove the extra moisture, the sample was then negatively stained with freshly prepared 2% aqueous uranyl acetate solution to enhance the imaging contrast. The substrate was allowed to air dry before observation at room temperature. The size and morphology of the exosomes were then visualized using a JEOL JEM1011 electron microscope operating at an accelerating voltage of 80 kV. TEM analysis indicated that the vesicles—prepared based

on the above-described protocol—consisted of mainly cup-shaped particles with multiple dimensions, and no indication of contamination with other exosomal particles or cellular organelles was observed (Figure S2).

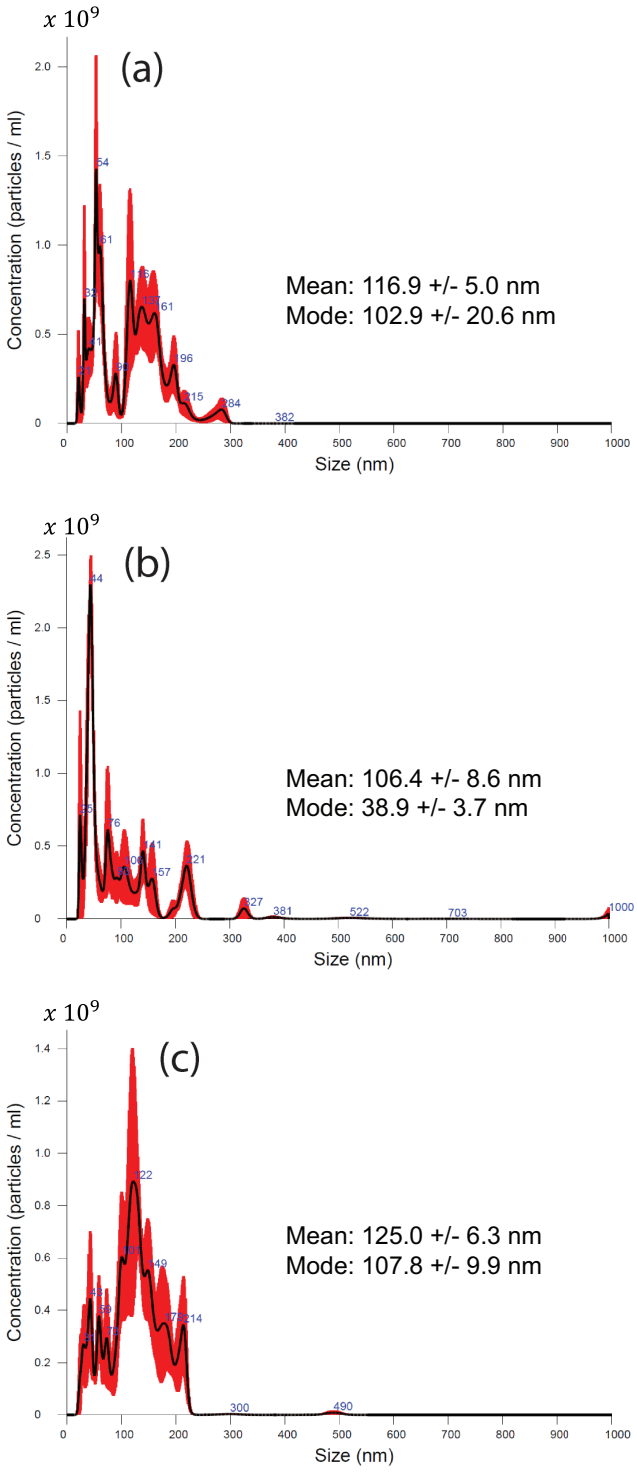

Figure S1: Size and concentration distribution of exosomes isolated from LM8 (a), HOS (b), and 143B (c) cell lines, respectively, determined by NTA using NanoSight analysis. NTA analysis revealed a mean size distribution of 116.9 +/-5.0 nm (a), 104.6 +/- 8.6 nm (b), and 125.0 +/- 6.3 nm (c) for the main exosome population. In various different measurements, the mean size of vesicles was measured in the range of 100 to 130 nm, which is consistent with the size of exosomes determined in previous studies using NTA.

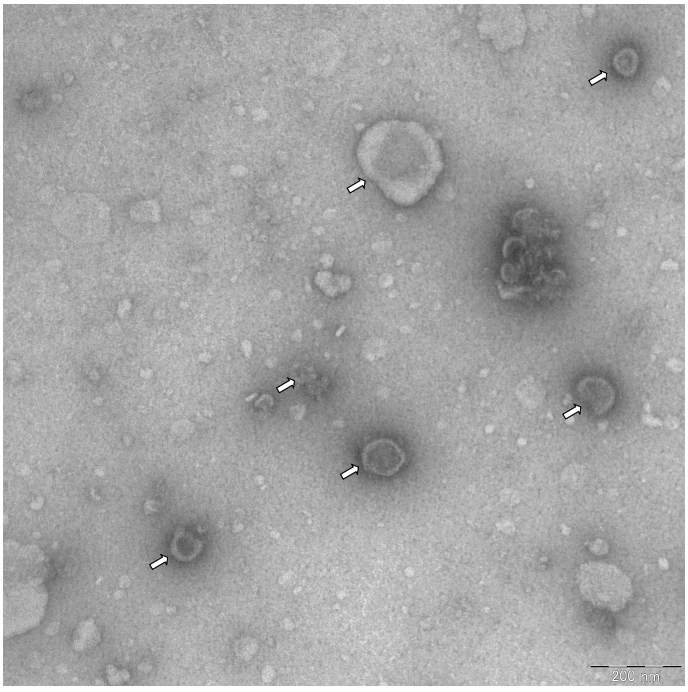

Figure S2: **TEM characterization of exosomes:** A typical electron micrograph of negatively stained vesicles derived from 143B cell lines. TEM analysis confirmed the presence of characteristic 2D cup-shaped, shrunken vesicles of various sizes. The results of TEM, furthermore, indicated that the vesicles—isolated based on the sample preparation protocol described in the main manuscript—consisted of mainly cup-shaped particles with multiple dimensions, and no indication of contamination with other exosomal particles or protein complexes were observed. Scale bar is 200 nm in length.

Additional experimental data

AFM images of ruptured exosomes in water

We have found that strong binding forces between exosomes and the underlying highly positively charged APTES-modified mica substrate can lead to a rupture of spherical vesicles. A rupture of spherical vesicles results in the formation of flattened-bilayer patches (Figure S3a). The average thickness of these exosomal lipid bilayers was about 4.5–5 nm (Figure S3b), which is in good agreement with the expected height of a supported lipid bilayer demonstrated by cryo-TEM on EVs from blood plasma.[2,3] This is also in good accordance with the values determined by AFM, cryo-TEM, and small-angle neutron scattering experiments on a DMPC liposome.[4–6] Following the vesicle rupture, we witnessed the appearance of fibrillar-like structures along with other exosomal content dispersed on the surface. In contrast, these fibrillar structures were not observed on a surface with intact exosomes. These fibrillar structures are presumably associated with the presence of nucleic acids, i.e., DNA or RNA. There is still an ongoing discussion on the presence of DNA content in exosomes in the literature.[7] The appearance of fibrillar structures on the surface in our AFM images, accompanied by the formation of lipid bilayer patches, provides strong evidence that these structures are exuded out the membrane surface (Figures S3c and S3d). We performed high-resolution AFM imaging and force mapping to determine the detailed structure and biochemical identity of these exosomal entities (Figures. S3e and S3f). The grooves of these DNA-like structures were resolved in high-resolution AFM images. We identify a distance between bright protruding features of 1.5-1.8 nm, which can be associated with the minor grooves of the fibrillar-like structures. However, it isn't easy to judge whether this structure is DNA or RNA. Further studies will be needed to determine the identity of these structures.

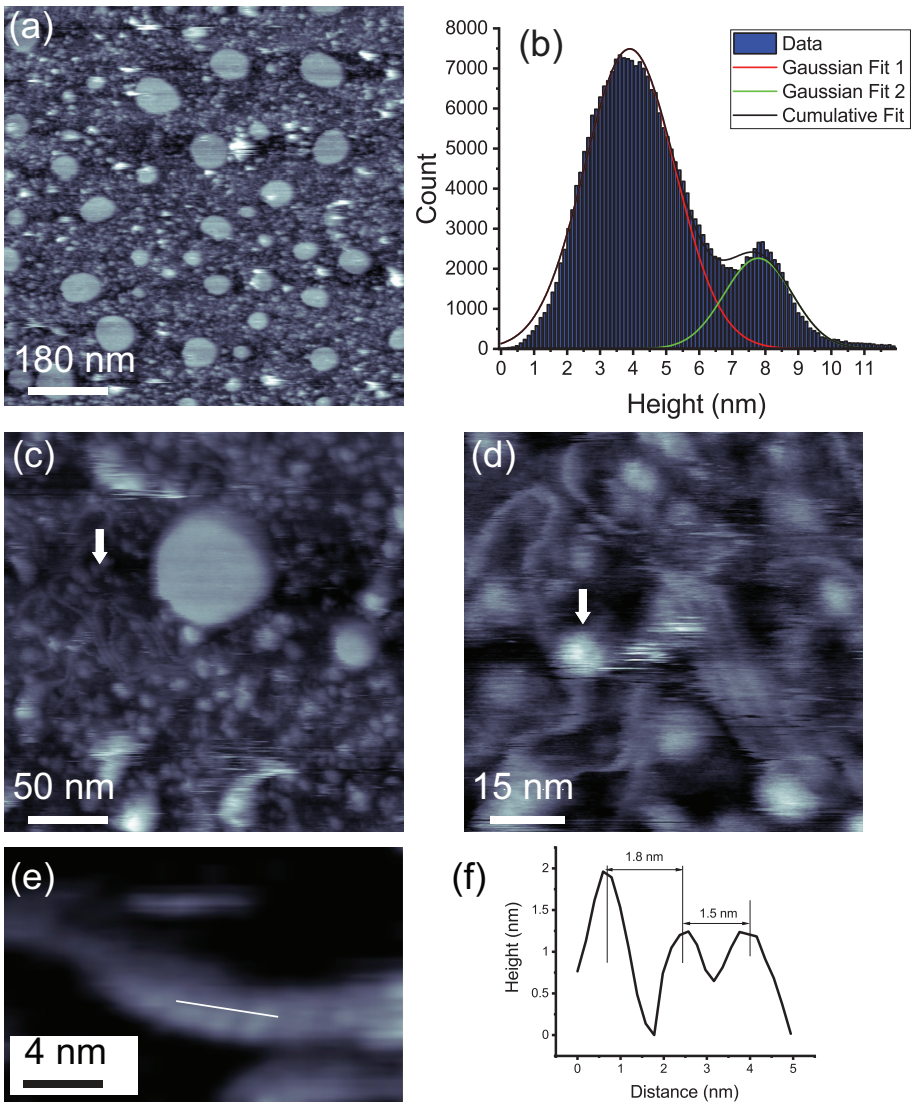

Figure S3: **AFM images of ruptured exosomes**. (a) An AFM image showing lipid bilayer of ruptured exosomes from 143B cell lines. Due to strong substrate-vesicle interactions or adhesion, the round (spherical) vesicle was fully collapsed into a single bilayer structure. (b) Histogram showing the height distribution of the ruptured membranes on the APTES-modified mica substrate in water. Two peaks are apparent in the histogram. The peak on the left (red) is due to the underlying substrate, while the one on the right (green) corresponds to the membrane patch. A height difference of approximately 4 nm can be seen between two peaks, which is in good agreement with the expected height of a supported lipid bilayer, as demonstrated by cryo-TEM on EVs from blood plasma.[2,3] (c-d) An AFM image of a surface region, showing the presence of fibrillar structures. Following the vesicle rupture, we witnessed the appearance of fibrillar-like structures and other exosomal contents dispersed on the surface. (e) High-resolution AFM image showing grooves of DNA-like structures. (f) Height profile taken along the white line shown in panel e. We identify a distance between bright protruding features of 1.5-1.8 nm, which can be associated with the minor grooves of the fibrillar-like structures. However, it is difficult to say whether these structures are DNA or RNA.

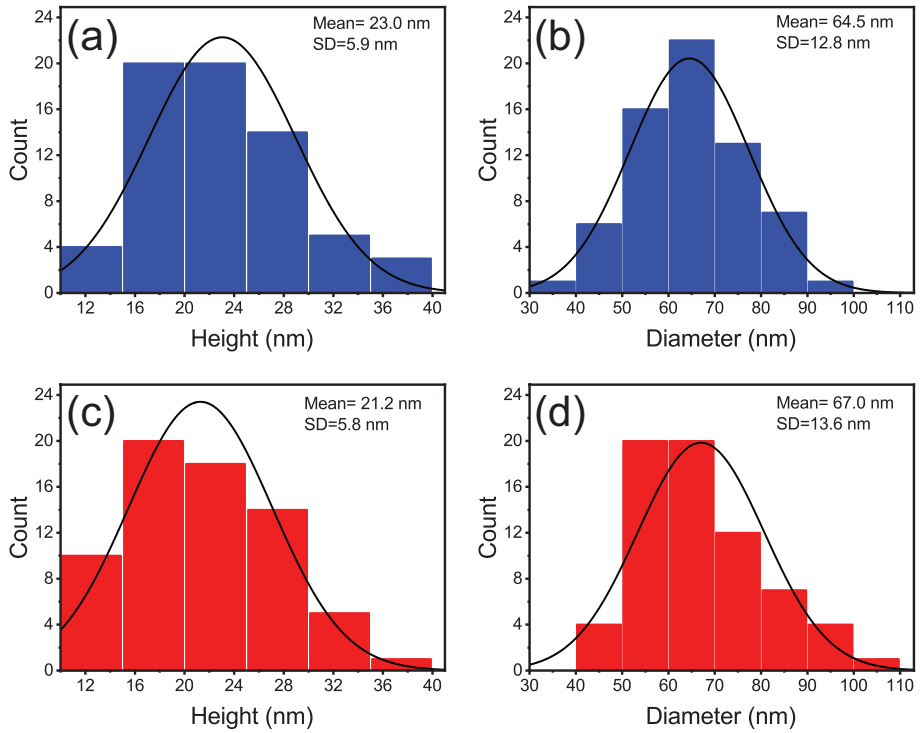

Figure S4: **Size distribution comparison of exosomes isolated from HOS (a-b) and 143B (c-d) cell lines, respectively, determined by AFM**. Height (a) and width (diameter) (b) distribution of HOS cell-derived exosomes immobilized on an APTES-modified mica in water. Height (c) and diameter (d) distribution of 143B cell-derived exosomes immobilized on an APTES-modified mica in water. The solid black curves represent the Gaussian fitting. The mean height values are 23 $\pm$ 5.9 and 21.2 $\pm$ 5.8 nm for HOS and 143B cell-derived exosomes, respectively. The mean diameter values are 64.5 $\pm$ 12.8 and 67.0 $\pm$13.6 nm for HOS and 143B cell-derived exosomes, respectively. The average size and size distribution of vesicles were in good agreement with the NTA analysis. The particles' average size is almost equal for HOS cell- and 143B cell-derived exosomes, and is identical to the average size of LM8 cell-derived exosomes, as reported in Figure 2d of the main manuscript. For all the cell lines, the particle sizes determined by AFM showed a bimodal distribution.

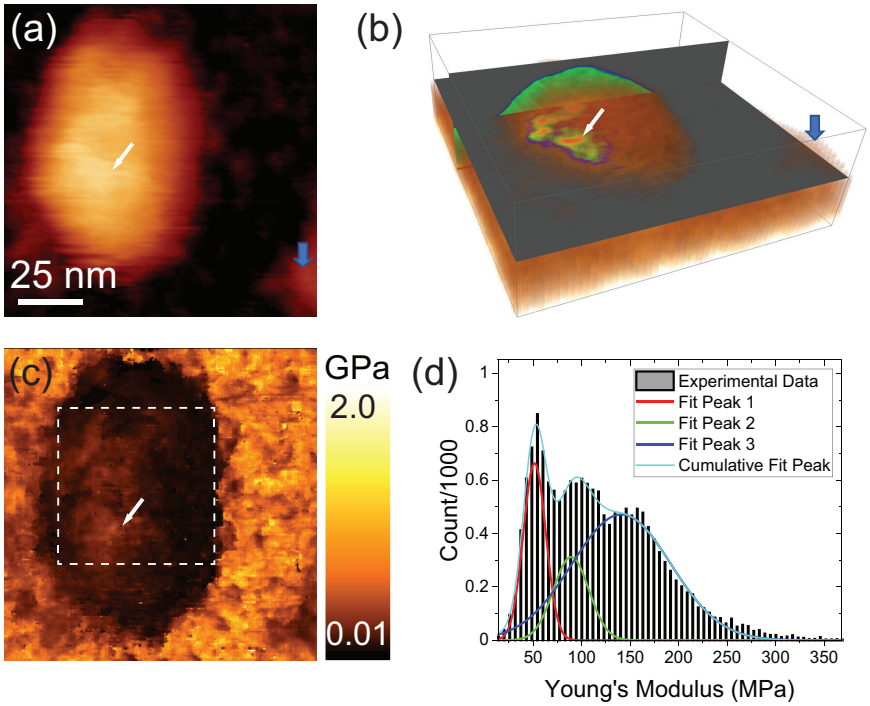

Figure S5: **Mechanical property map of exosomes**: Topography (a) and corresponding force (b) and Young's modulus map (c) of an exosome derived from the LM8 cell line, as also shown in Figure 5 of the main manuscript. The distinct domains highlighted with arrows were clearly resolved in 3D force and Young's modulus map. (d) Distribution of Young's moduli showing additional peaks at lower modulus values, as compared with the distribution shown in Figure 5d of the main manuscript. The histogram was obtained from the region covering an area of approximately 60 $\times$ 60 nm^2 with 128 $\times$ 128 pixels resolution, including almost all of the area enclosing an individual exosome. The cumulative curve of the histogram can be decomposed into three peaks. The solid red, blue, and green lines represent the fitted Gaussian functions. While at the very top region of the vesicle (with 64 $\times$ 64 pixels), the distributions are generally unimodal and can be fitted by a Gaussian function (see Figure 5d in the main manuscript), the distributions—constructed from the relatively larger surface area with 128 $\times$ 128 pixels, are multi-modal and can be fitted by three Gaussian functions. The mean values of these three Gaussian distributions are 51.40 $\pm$ 0.46 MPa, 89.10 $\pm$ 1.38 MPa, and 140.92 $\pm$ 2.73 MPa, respectively. The distribution with a higher value of Young's modulus corresponds to the central region of the vesicle. The Young's modulus distribution with fitted three Gaussian functions reflects the local mechanical heterogeneity of the vesicle surface.

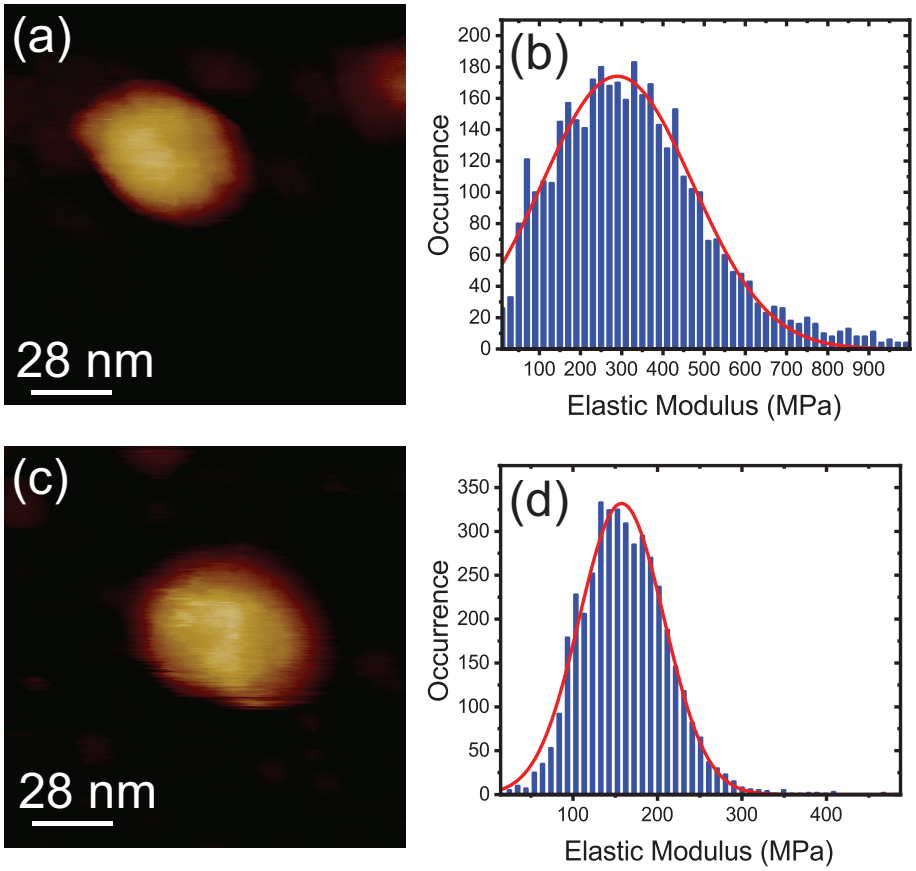

Figure S6: **Representative Young's modulus distributions obtained from 143B and HOS cell-derived-exosomes**. AFM topography images of (a) 143B and (c) HOS cell-derived exosomes immobilized on an APTES-modified mica, acquired in water. Corresponding histograms show the distributions of Young's moduli for (b) 143B and (d) HOS cell-derived exosomes. The solid red lines represent the Gaussian fitting. The measured average Young's modulus values are 289.3 $\pm$ 183.0 and 157.4 $\pm$50.1 MPa for 143B- and HOS-cell-derived exosomes, respectively.

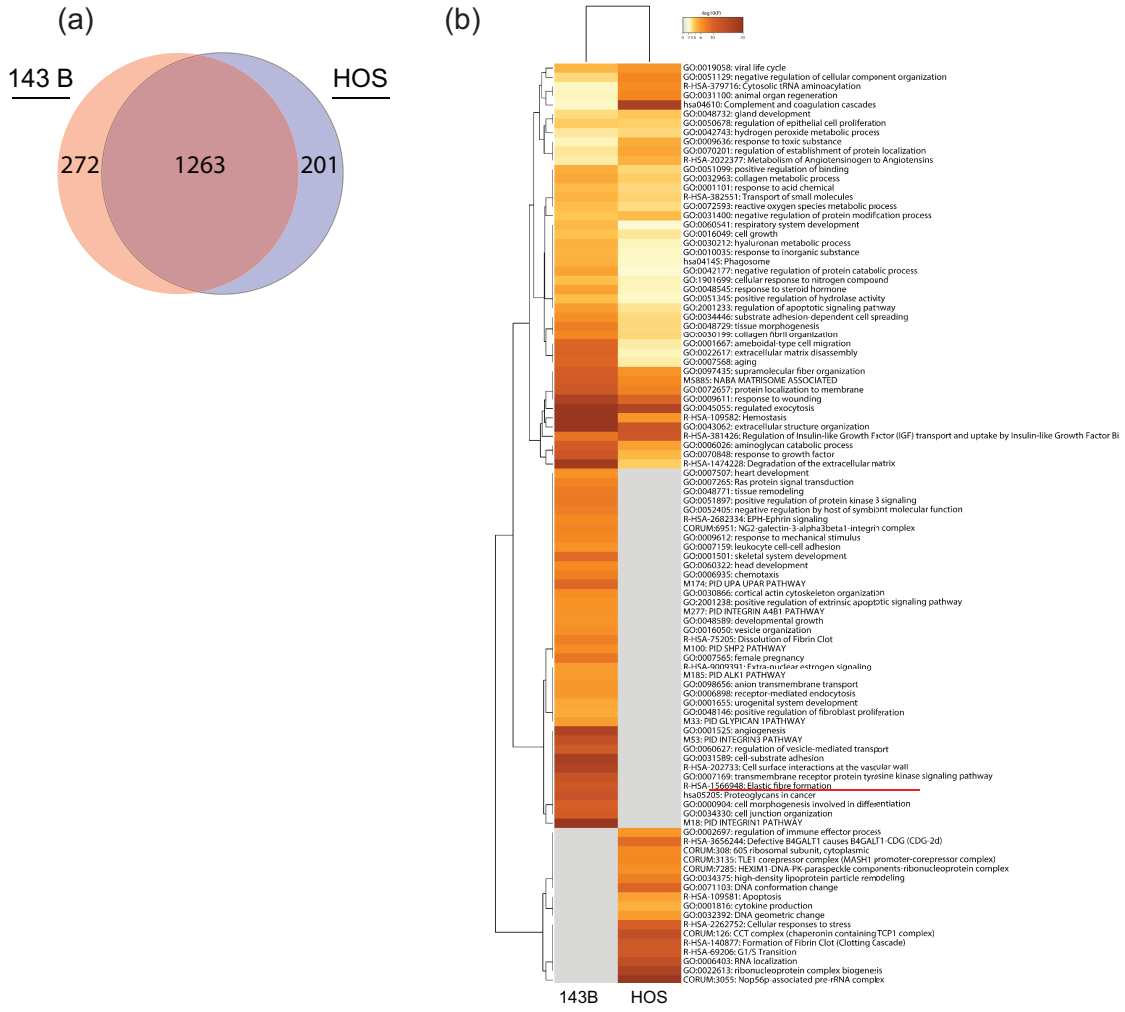

Figure S7: **Proteomic profiling of exosomes derived from HOS and 143B cell lines**. (a) Venn diagram showing the distribution of identified proteins, indicating the common and unique proteins for each exosome. LC-MS analysis identified a total of 1535 proteins in 143B cell-derived exosomes, and 1464 proteins in HOS cell-derived exosomes. While 272 proteins were included only in 143B exosomes, 201 were unique to HOS exosomes, and 1263 were shared between them. (b) Among the proteins identified by LC-MS analysis, we extracted 143B or HOS exosomal-specific proteins that were present by over five-fold more in one cell type compared to the other. Overall, 345 and 428 proteins were identified as 143B and HOS exosomal-specific proteins, respectively. These proteins were then subjected to gene ontology (GO) enrichment analysis to determine their molecular and biological functions using Metascape analysis software. Red line shows protein groups involved in elastic fiber formation.

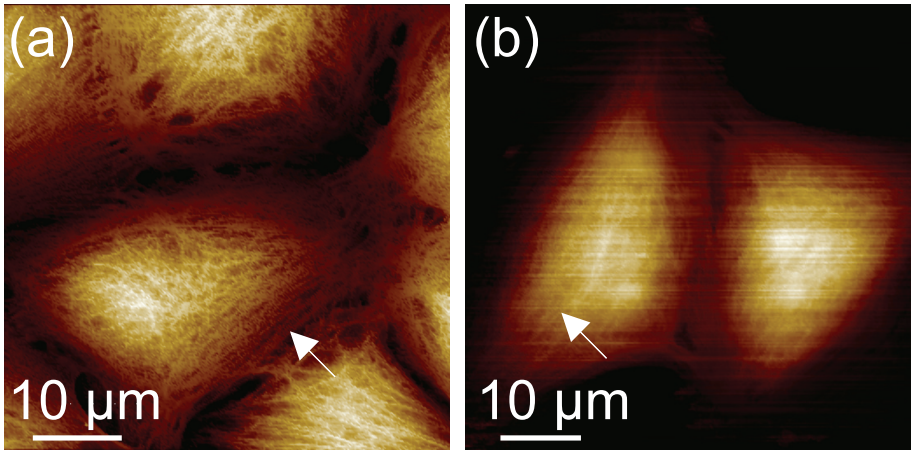

Figure S8: AFM topography images of live HOS (a) and 143B (b) cells seeded on a Petri dish, acquired with a sharp tip in CO_2-independent medium (Leibovitz's L-15) at 37°C. The arrows indicate the fibrous structures, probably actin stress fibers. The HOS cells exhibited a greater number of actin stress fibers than 143B cells. These entangled fibrillar networks have been demonstrated to confer a high mechanical strength to living cells.[8] We anticipate that a high density of these fibers may provide a higher elastic modulus to the HOS cells compared to the 143B cells. We note that these stiffer subcellular features become apparent when the applied loading force is increased.

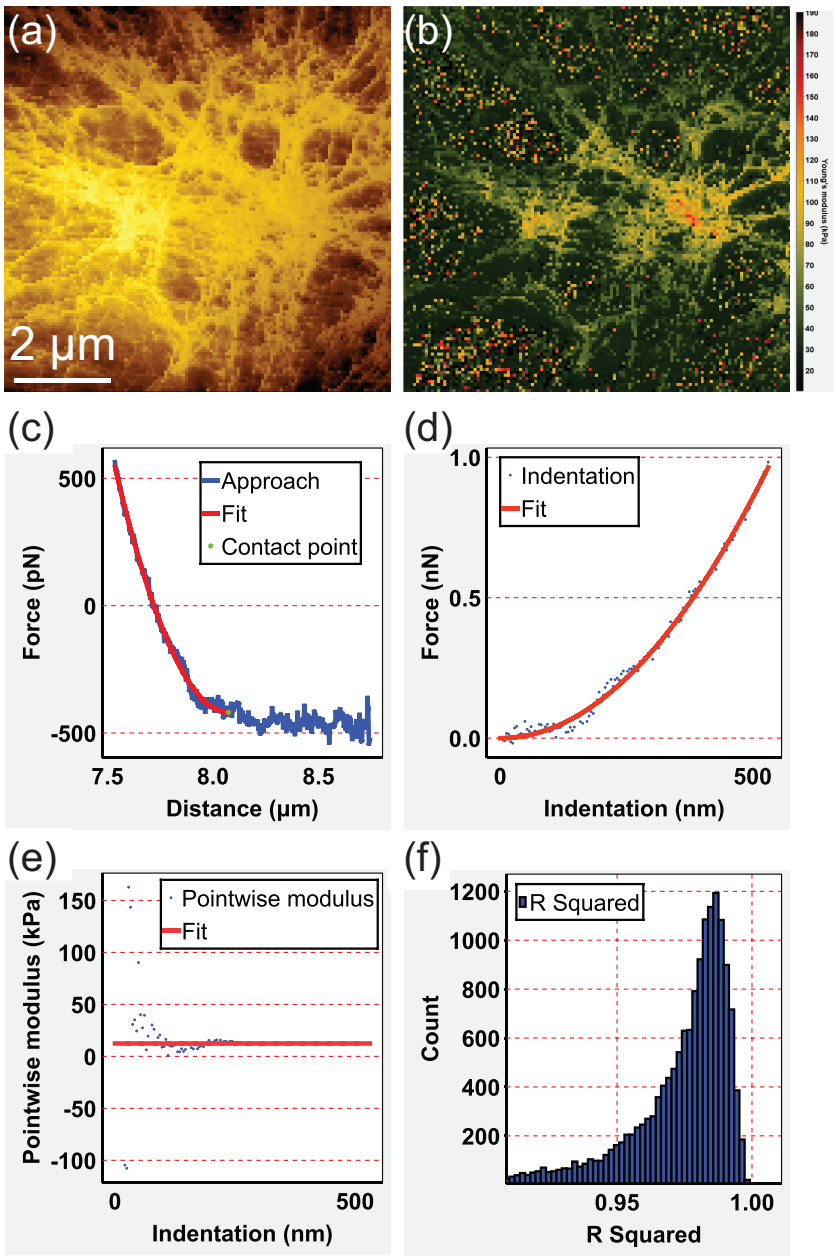

Figure S9: **Extraction of mechanical properties of live HOS and 143B cells**. A representative AFM topography ($8 \times 8\ \mu m^2$) (a) and corresponding Young's modulus map (b) of living HOS cell, acquired with a sharp tip in CO_2-independent medium (Leibovitz's L-15) at 37°C. The Young's modulus map was obtained from a grid of 128×128 force curves recorded on the cell's nucleus. The regions with fibrous structures in panel a correspond to the high Young modulus values in panel b, supporting the idea that the entangled network of these fibers contributes to the increased cells stiffness. A representative force vs. distance (c) and corresponding force vs. indentation (d) curves with the fitted curves (red) taken on a HOS cell. The green dot indicates the position of the contact point. A Sneddon model fit was used to calculate the Young's modulus. (e) Pointwise modules vs. indentation plot, pointing out the fact that a sufficiently large enough indentation depth is required to attain a plateau region where the Young's modulus value is independent of the indentation depth. A plateau region was identified in an indentation range of 300-500 nm above the nucleus of a HOS cell. (f) Histogram showing the R^2 values for the Sneddon model fits of all data points in the entire force map.

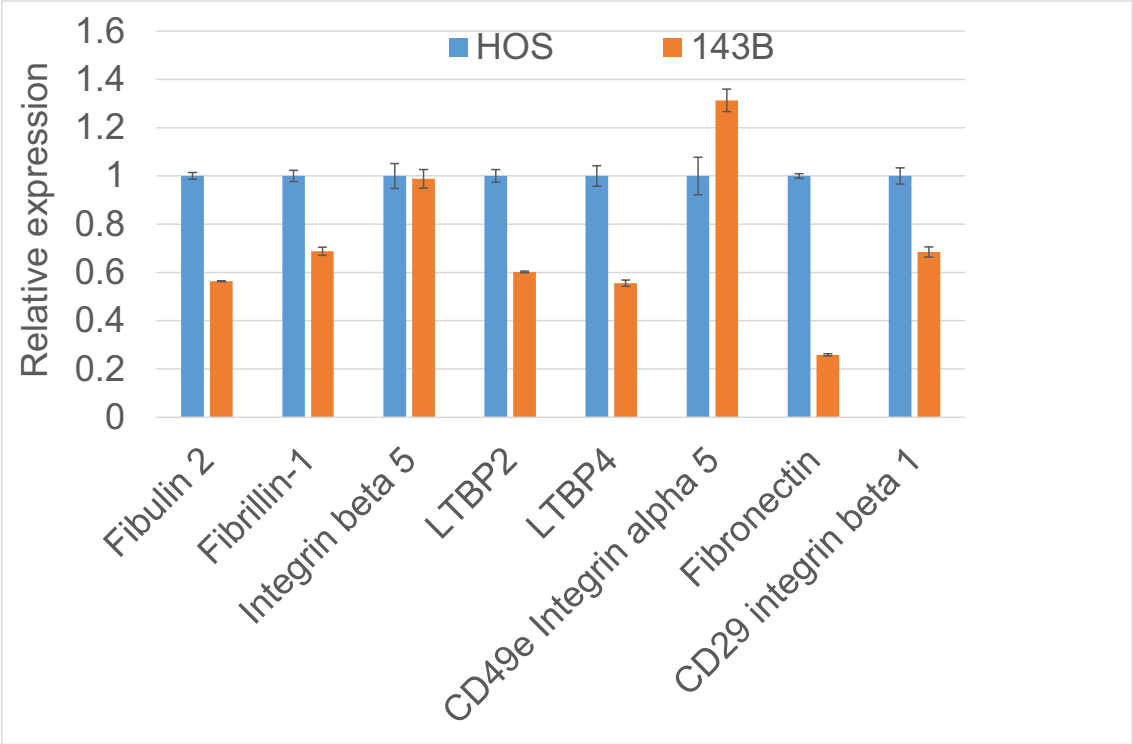

Figure S10: **Proteomic profiling of parental cells that secrete HOS- and 143B-exosomes**. Cell-based ELISA analysis of several selected proteins expression in HOS and 143B cells. Except integrin beta 5 and alpha 5, elastic-fiber associated proteins were more highly expressed in HOS cells than in 143B cells.

References

1. Chernyshev, V. S.; Rachamadugu, R.; Tseng, Y. H.; Belnap, D. M.; Jia, Y.; Branch, K. J.; Butterfield, A. E.; Pease, L. F.; Bernard, P. S.; Skliar, M. Size and shape characterization of hydrated and desiccated exosomes. *Analytical and Bioanalytical Chemistry* **2015**, *407*, 3285–3301.

2. Arraud, N.; Linares, R.; Tan, S.; Gounou, C.; Pasquet, J.-M.; Mornet, S.; Brisson, A. R. Extracellular vesicles from blood plasma: determination of their morphology, size, phenotype and concentration. *Journal of Thrombosis and Haemostasis* **2014**, *12*, 614–627.

3. Yuana, Y.; Koning, R. I.; Kuil, M. E.; Rensen, P. C. N.; Koster, A. J.; Bertina, R. M.; Osanto, S. Cryo-electron microscopy of extracellular vesicles in fresh plasma. *Journal of Extracellular Vesicles* **2013**, *2*, 21494.

4. Winzen, S.; Bernhardt, M.; Schaeffel, D.; Koch, A.; Kappl, M.; Koynov, K.; Landfester, K.; Kroeger, A. Submicron hybrid vesicles consisting of polymer-lipid and polymer-cholesterol blends. *Soft Matter* **2013**, *9*, 5883–5890.

5. Kucerka, N.; Kiselev, M.; Balgavý, P. Determination of bilayer thickness and lipid surface area in unilamellar dimyristoylphosphatidylcholine vesicles from small-angle neutron scattering curves: A comparison of evaluation methods. *European biophysics journal : EBJ* **2004**, *33*, 328–34.

6. Zhou, J.; Liang, D.; Contera, S. Effect of intra-membrane C60 fullerenes on the modulus of elasticity and the mechanical resistance of gel and fluid lipid bilayers. *Nanoscale* **2015**, *7*, 17102–17108.

7. Takahashi, A.; Okada, R.; Nagao, K.; Kawamata, Y.; Hanyu, A.; Yoshimoto, S.; Takasugi, M.; Watanabe, S.; Kanemaki, M. T.; Obuse, C.; Hara, E. Exosomes maintain cellular homeostasis by excreting harmful DNA from cells. *Nature Communications* **2017**, *8*, 15287.

8. Burla, F.; Mulla, Y.; Vos, B. E.; Aufderhorst-Roberts, A.; Koenderink, G. H. From mechanical resilience to active material properties in biopolymer networks. *Nature Reviews Physics* **2019**, *1*, 249–263.